

Time-dependent current into and through multilevel parallel quantum dots in a photon cavity

Vidar Gudmundsson,^{1,*} Nzar Rauf Abdullah,² Anna Sitek,^{1,3}
Hsi-Sheng Goan,^{4,5,†} Chi-Shung Tang,^{6,‡} and Andrei Manolescu^{7,§}

¹*Science Institute, University of Iceland, Dunhaga 3, IS-107 Reykjavik, Iceland*

²*Physics Department, College of Science, University of Sulaimani, Kurdistan Region, Iraq*

³*Department of Theoretical Physics, Wrocław University of Science and Technology, 50-370 Wrocław, Poland*

⁴*Department of Physics and Center for Theoretical Sciences,
National Taiwan University, Taipei 10617, Taiwan*

⁵*Center for Quantum Science and Engineering, National Taiwan University, Taipei 10617, Taiwan*

⁶*Department of Mechanical Engineering, National United University, Miaoli 36003, Taiwan*

⁷*School of Science and Engineering, Reykjavik University, Menntavegur 1, IS-101 Reykjavik, Iceland*

We analyze theoretically the charging current into, and the transport current through, a nanoscale two-dimensional electron system with two parallel quantum dots placed in a photon cavity. A plunger gate is used to place specific many-body states of the interacting system in the bias window defined by the external leads. We show how the transport phenomena active in the many-level complex central system strongly depend on the gate voltage. We identify a resonant transport through the central system as the two spin components of the one-electron ground state are in the bias window. With two-electron states in the bias window we observe a more complex situation with intermediate radiative and nonradiative relaxation channels leading to a steady state with a weak nonresonant current caused by inelastic tunneling through the two-electron ground state of the system.

Various properties of nanoscale electron and spin systems in microwave cavities are presently the focus point of many researchers. Just to mention some; photon emission from a cavity-coupled double quantum dot caused by an electron transport through it has been reported,¹ and the manipulation of spin qubits in cavities has gained paramount interest.^{2,3}

Investigations of transport of electrons through solid state electronic systems placed in photon cavities are gaining attention. Partially, due to the obvious connection to efforts to achieve quantum computation in a solid state system, and partially due to the interest to study fundamental light-matter interactions in a system expected to be highly tunable and offer increased sensitivity of measurements. In several cases the electronic systems have been single or multiple quantum dots created with InAs,² GaAs,^{4,5} carbon nanotubes,³ or graphene,⁶ and very recently in SiGe heterostructures.⁷

Experiments have been reported on carbon nanotube quantum dots in a planar microwave cavity coupled to external fermionic or superconducting leads. The sensitivity of the measurements due to the cavity allows for the detection of a photon assisted current of 0.3 pA corresponding to the mean photon number in the cavity being 120,^{8,9} a current much lower than is common in measurements of photon assisted tunneling through quantum dots, when not placed in a cavity.¹⁰

Numerous models have been presented for transport and processes in cavity-quantum electrodynamics systems,^{11–13} and time dependent electron transport through nano electron systems in a photon cavity in the transient,¹⁴ or in the long time regime on the way towards the steady state.¹⁵

Here, we present results concentrating on the charging

current of, or the transport current through, a system of two multilevel parallel quantum dots embedded in a short two-dimensional quantum wire placed in a photon cavity with one mode. We use a recently developed Markovian version of the model to analyze the transport current in the long time limit in Liouville space.^{15,16} Alternative scheme has been employed by Marino and Diehl that transform a Markovian master equation into a dynamical field theoretical model that they subject to a Keldysh functional renormalization to investigate nonequilibrium phase transitions in driven open systems.¹⁷

As we are describing transport through a multilevel system including both the para- and diamagnetic part of the electron-photon interaction¹⁸ we will not be limited to couple any particular two levels of the electron system resonantly with the cavity photon mode, but we are rather interested in analyzing all underlying relaxation channels. Experiments on transport through electron systems in a photon cavity are usually not performed with time resolution, but in externally photon pumped cavities.⁹ Computational results from time resolved models of the underlying processes can serve as a basis for understanding and interpreting experimental results with growing complexity of the systems, as will be discussed below.

Our goal is to describe complex nanoscale electron systems placed in the photon cavity, and that requires a special attention to the geometry of the system and all interactions and couplings. We use a model with state dependent coupling tensor between the central electron system and the semi-infinite external leads and a step-wise introduction of complexity (interactions and components) together with appropriate truncation of the ensuing many-body spaces at each step.^{14,19}

I. THE MODEL

We consider a short two-dimensional quantum wire incorporating two parallel quantum dots which is placed in a photon cavity. We will call this device the central system. The short quantum wire, and indirectly the entire central system, is weakly coupled to two external leads, the left (L) and the right (R) leads, acting as electron reservoirs. The coupling opens up the central system to electron transport through it at time $t = 0$. Below we first establish details of the central system of strongly coupled electrons and photons and review its properties. Then we describe the master equation formalism used to model the time-dependent electron transport through the open central system.

A. The central system

We consider a short two-dimensional quantum wire with two parallel quantum dots placed in a photon cavity. The potential energy landscape can be described by the formula

$$V(x, y) = \left[\frac{1}{2} m^* \Omega_0^2 y^2 + V_d \sum_{i=1}^2 \exp \{ -(\beta x)^2 + \beta^2 (y - d_i)^2 \} \right] \times \theta \left(\frac{L_x}{2} - x \right) \theta \left(\frac{L_x}{2} + x \right), \quad (1)$$

with $\hbar\Omega_0 = 2.0$ meV, $V_d = -6.5$ meV, $\beta = 0.03$ nm⁻¹, $d_1 = -50$ nm, $d_2 = +50$ nm, $L_x = 150$ nm, and θ is the Heaviside step function. The potential is shown in Fig. 1. The first line in Eq. (1) describes the parabolic confinement of the short quantum wire in the y -direction, perpendicular to the transport direction.

The central system can contain several photons (0-16) and few electrons (0-4) and is best described by a many-body formalism. The interactions of its constituents are accounted for via a configuration interaction (CI) approach (also known as exact numerical diagonalization).¹⁹ We assume GaAs parameters, $\kappa = 12.4$, $m^* = 0.067m_e$, and $g^* = -0.44$. The Hamiltonian operator for the central system in terms of the field operators is

$$H_S = \int d^2r \psi^\dagger(\mathbf{r}) \left\{ \frac{\pi^2}{2m^*} + V(\mathbf{r}) \right\} \psi(\mathbf{r}) + H_{\text{EM}} + H_{\text{Coul}} - \frac{1}{c} \int d^2r \mathbf{j}(\mathbf{r}) \cdot \mathbf{A}_\gamma - \frac{e}{2m^*c^2} \int d^2r \rho(\mathbf{r}) A_\gamma^2, \quad (2)$$

with

$$\boldsymbol{\pi} = \left(\mathbf{p} + \frac{e}{c} \mathbf{A}_{\text{ext}} \right), \quad (3)$$

where \mathbf{A}_{ext} is a classical vector potential generating an external homogeneous small magnetic field $B = 0.1$ T

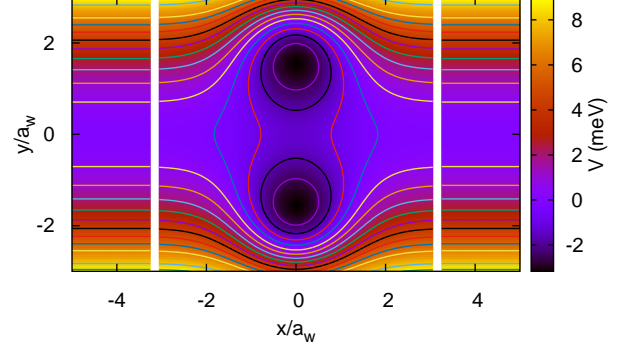


FIG. 1. The central system connected to the parabolically confined semi-infinite external leads. The common confinement energy of the leads and the central system $\hbar\Omega_0 = 2.0$ meV, and the small perpendicular external magnetic field $B = 0.1$ T define a characteristic length $a_w = 23.8$ nm.

along the z -axis perpendicular to the plane of the two-dimensional semiconductor inserted in order to break spin and orbital degeneracies to enhance accuracy of the results. H_{EM} is the Hamiltonian for the single cavity photon mode with energy $\hbar\omega = 0.8$ meV, and the electron-electron static Coulomb repulsion is represented by H_{Coul} written in terms of four field operators and a spatially dependent Coulomb kernel.¹⁹ The quantized vector potential of the cavity photon field is \mathbf{A}_γ . The last two terms of the Hamiltonian (2) stand for the para- and the diamagnetic electron-photon interactions, respectively, necessary since we will consider photon energy that might, or might not be, close to a transition resonance between particular electron states.^{18,20} The charge and the charge-current density operators are

$$\rho = -e\psi^\dagger\psi, \quad \mathbf{j} = -\frac{e}{2m^*} \{ \psi^\dagger (\boldsymbol{\pi}\psi) + (\boldsymbol{\pi}^*\psi^\dagger) \psi \}. \quad (4)$$

The external magnetic field, $B = 0.1$ T, and the parabolic confinement energy of the leads and the central system $\hbar\Omega_0 = 2.0$ meV, lead together with the cyclotron frequency $\omega_c = ((eB)/(m^*c))$ to an effective characteristic frequency $\Omega_w = (\omega_c^2 + \Omega_0^2)^{1/2}$ and an effective magnetic length $a_w = (\hbar/(m^*\Omega_w))^{1/2}$.

We consider a rectangular photon cavity $(x, y, z) \in \{[-a_c/2, a_c/2] \times [-a_c/2, a_c/2] \times [-d_c/2, d_c/2]\}$ with the short two-dimensional quantum wire centered in the $z = 0$ plane. Using the Coulomb gauge the polarization of the electric field is parallel to the transport in the x -direction by selecting the TE₀₁₁ mode, or perpendicular by selecting the TE₁₀₁ mode. In terms of the creation and annihilation operators, a^\dagger and a , for cavity photons the quantized vector potential is

$$\mathbf{A}_\gamma(\mathbf{r}) = \begin{pmatrix} \hat{\mathbf{e}}_x \\ \hat{\mathbf{e}}_y \end{pmatrix} \mathcal{A} \{ a + a^\dagger \} \begin{pmatrix} \cos\left(\frac{\pi y}{a_c}\right) \\ \cos\left(\frac{\pi x}{a_c}\right) \end{pmatrix} \cos\left(\frac{\pi z}{d_c}\right), \quad (5)$$

for the TE_{011} and TE_{101} modes, respectively. The strength of the vector potential, \mathcal{A} , determines the coupling constant $g_{\text{EM}} = e\mathcal{A}\Omega_w a_w/c$, here set to 0.05 meV, leaving a dimensionless polarization tensor

$$g_{ij} = \frac{a_w}{2\hbar} \{ \langle i | \hat{\mathbf{e}} \cdot \boldsymbol{\pi} | j \rangle + \text{h.c.} \}, \quad (6)$$

where $|i\rangle$ and $|j\rangle$ are single-electron states of the short two-dimensional quantum wire. Latin indices are used for the single-electron states, and Greek for the many body states to be described below.

In order to find the energy spectrum and the states of the closed central system we use a stepwise scheme of exact numerical diagonalizations and truncations:¹⁹ First, the single-electron states of the system are used to build a Fock-space for 0-4 noninteracting electrons $\{|\mu\rangle\}$. This space is truncated well above the bias window. Second, the Hamiltonian of the Coulomb interacting electrons is diagonalized in the Fock basis creating a new Fock-space of Coulomb interacting electrons $\{|\mu\rangle\}$. Third, the Fock-space of the Coulomb-interacting electrons is used to build a many-body basis for Coulomb interacting electrons and cavity photons by a tensor product of $\{|\mu\rangle\}$ and the eigenstates $|N\rangle$ of the photon number operator. This new basis is used to diagonalize the full Hamiltonian of the central system (2) obtaining a new Fock-space of interacting electrons and photons $\{|\tilde{\mu}\rangle\}$, with pure photon states and cavity-photon dressed electron states. This construction is reminiscent and parallel to the possible construction of a Green function for the system (not done here), where one starts with a noninteracting Green function, and in a stepwise fashion dresses it with the Coulomb and the photon interactions through the Dyson equation. The construction here is entirely carried out in functional spaces in a grid-free manner.

The many-body energy spectra versus the plunger gate voltage V_g for the central system are presented in Fig. 2 for x -polarization of the cavity photon field, and in Fig. 3 for y -polarization. In both cases we indicate with a color coding the electron content (an integer in the closed system) in the left panel of the figure, and the photon number in the right panel. Without the electron-photon interaction the photon number is an integer, but the interaction does not conserve the number of photons. We will come back to this fact below. The dressed electron states do thus not contain an exact photon number and we can not refer to one- or two-photon replicas of an electron state, but as the replica concept is useful we refer to the first or second replica of a certain electron state.

For our parameters here we use 16 photon states. In our experience the convergence with respect to the photon basis is not critical, but instead the number of electron states is, as photon dressing in the strong coupling regime leads to increased polarization or spreading of the charge of a state.²¹

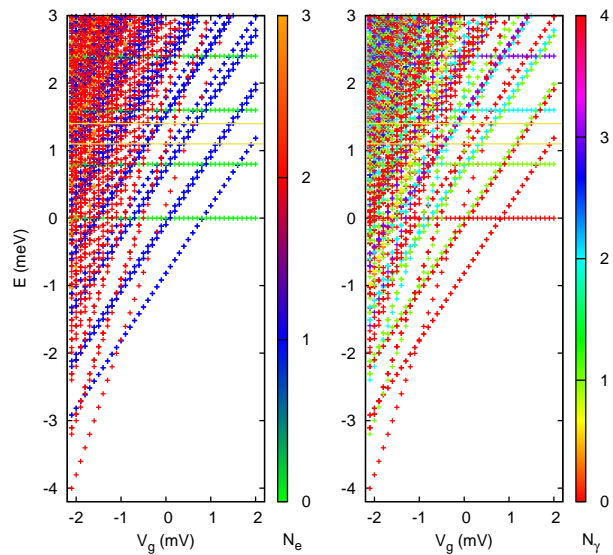


FIG. 2. Energy spectrum for x -polarized cavity photons versus plunger gate voltage V_g . Electron number (left panel), and the mean photon number (right panel) is color coded into the states. $\hbar\omega = 0.8$ meV, and $g_{\text{EM}} = 0.05$ meV.

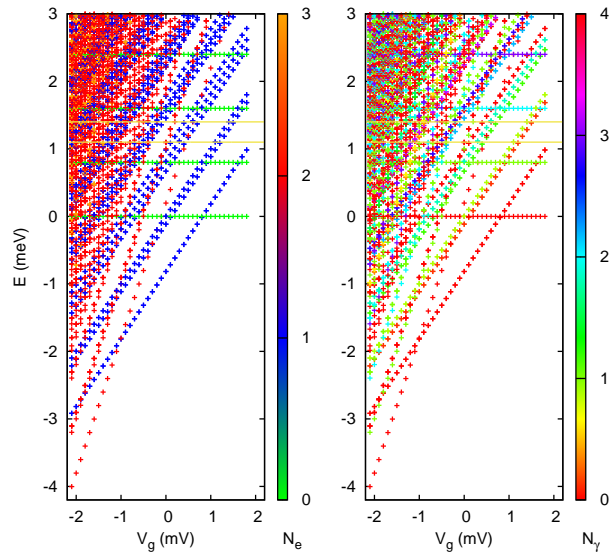


FIG. 3. Energy spectrum for y -polarized cavity photons versus plunger gate voltage V_g . Electron number (left panel), and the mean photon number (right panel) is color coded into the states. $\hbar\omega = 0.8$ meV, and $g_{\text{EM}} = 0.05$ meV.

B. Coupling to the leads – time evolution

The central system is weakly coupled to external leads and opened up to electron transport through it at time $t = 0$. The semi-infinite leads are parabolically confined and are in the same perpendicular classic weak magnetic field as the central system. In our calculations we include 4 of their subbands. The weak coupling is described by

the Hamiltonian^{22,23}

$$H_T(t) = \sum_{i,l} \chi(t) \int dq \left\{ T_{qi}^l c_{ql}^\dagger d_i + (T_{qi}^l)^* d_i^\dagger c_{ql} \right\}, \quad (7)$$

where d_i is the annihilation operator for an electron in the single-electron state of the central system labeled with i , and c_{ql}^\dagger is the creation operator for an electron in lead l with momentum and subband index labeled by the composite index q . The coupling tensor T_{qi}^l describes the coupling between these single-electron states of lead l and the central system, and depends on the geometrical form of the corresponding wave functions in the contact area extending approximately a_w into each subsystem.^{19,23} The remaining overall coupling constant to the leads is $g_{LR} a_w^{3/2} = 0.124$ meV. The switching of the coupling is determined by the Heaviside unit step function of time, at $t = 0$. Before the coupling there exist no correlations between the leads, or the leads and the central system.

The time evolution after the coupling of the leads and the central system can be described by the Liouville-von Neumann equation for the density operator of the system

$$\partial_t \rho = \mathcal{L} \rho, \quad (8)$$

where, \mathcal{L} is the Liouville operator, defined by the commutator

$$\mathcal{L} \rho = -i/\hbar [H, \rho], \quad (9)$$

with ρ the density operator of the total system, describing the dynamic state of both the leads and the central system. As the energy spectra of the leads (the electron reservoirs) are dense, we have in earlier publications resorted to applying a formalism of Nakajima²⁴ and Zwanzig²⁵ in which the dynamics of the whole system is projected on the central system leading to a generalized master equation (GME)²¹

$$\partial_t \rho_S(t) = -\frac{i}{\hbar} [H_S, \rho_S(t)] - \frac{1}{\hbar} \int_0^t dt' K[t, t'; \rho_S(t')] \quad (10)$$

for the reduced density operator $\rho_S(t)$ describing properties of the central system under influence of the external leads, and defined by tracing out variables of the leads $\rho_S(t) = \text{Tr}_{LR} \{\rho(t)\}$. The dissipative integral kernel, K , is constructed using terms of the coupling Hamiltonian (7) up to second order, but the integro-differential form of the GME guarantees higher order terms in the solution of the elemental type already present in K .

The solution to Eq. (10) can be found by numerical integration and iterations.^{22,23} However, for the $N = 120$ states needed here for the transport calculations in the photon dressed basis $\{|\tilde{\mu}\rangle\}$, it is not feasible to integrate the GME in time much farther than 1000 ps. To go beyond that we have made a Markovian approximation to the GME (10) avoiding any further approximations and using the Kronecker tensor product and vectorization

of matrices to map the equation from the Fock space of states to Liouville space of transitions.^{15,16}

In the N^2 -dimensional Liouville space²⁶ the linear equation of motion is^{27,28}

$$\partial_t \text{vec}(\rho_S) = \mathfrak{L} \text{vec}(\rho_S), \quad (11)$$

with \mathfrak{L} a general non-Hermitian operator with complex eigenvalues. The exact solution of Eq. (11) is¹¹

$$\text{vec}(\rho_S(t)) = \left\{ \mathfrak{U} \left[\exp \left(-\frac{i}{\hbar} \mathfrak{L}_{\text{diag}}(t) \right) \right] \mathfrak{B} \right\} \text{vec}(\rho_S(0)), \quad (12)$$

in terms of the left, \mathfrak{U} , and right, \mathfrak{B} , eigenvectors of \mathfrak{L} ,

$$\begin{aligned} \mathfrak{L} \mathfrak{B} &= \mathfrak{B} \mathfrak{L}_{\text{diag}}, \\ \mathfrak{U} \mathfrak{L} &= \mathfrak{L}_{\text{diag}} \mathfrak{U}, \end{aligned} \quad (13)$$

with the normalization condition

$$\begin{aligned} \mathfrak{U} \mathfrak{B} &= I \\ \mathfrak{B} \mathfrak{U} &= I. \end{aligned} \quad (14)$$

As the terms in \mathfrak{L} can be cleanly traced back to the left or the right lead with no mixed terms we can, as before,^{22,23} calculate the current from the left lead into the central system, I_L , and the current from the central system into the right lead, I_R , using the time-derivative of $\text{vec}(\rho_S(t))$ in the equation of motion (11) and its solution (12).

II. RESULTS

We explore the time dependent electron transport into and through the system for three different values of the plunger gate voltage, V_g . We start with $V_g = +2.0$ mV, when only the two spin components of the one-electron ground state are in the bias window, set by the chemical potentials of the left and right leads, $\mu_L = 1.4$ meV and $\mu_R = 1.1$ meV, respectively. We expect resonant transport through the system. In Figure 4 we show results for the mean electron and photon number in the central system for two initial states, totally empty system (0G), and only one photon in the central system (0G γ). In both cases the mean electron number rises quickly and remains constant just over 0.7. In the latter case (0G γ) the mean photon number vanishes on a longer time scale, and for the former case the mean photon number never gains a value visible in Fig. 4.

Not surprisingly the current for the two cases, shown, in Fig. 5, is approximately the same. For a short time the current is towards the central system from both leads (the right current, I_R , is negative in the beginning). After 10 ns the system seems to be in a steady state with the current flowing through the central system.

This view is not in agreement with the occupation of the many-body states of the central system shown in the upper panel of Fig. 6. There, we see for the former case

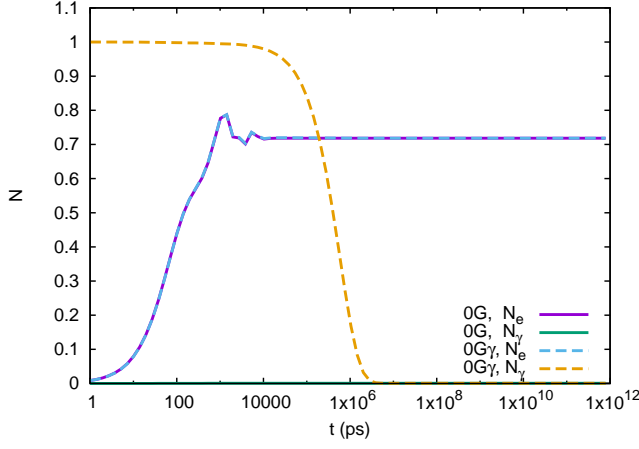


FIG. 4. Mean electron and photon numbers in the central system as a function of time for initially the vacuum state (0G), and one photon in the system (0G γ). x -polarized photons, $V_g = +2.0$ mV, $B = 0.1$ T, $\hbar\omega = 0.8$ meV, and $g_{EM} = 0.05$ meV.

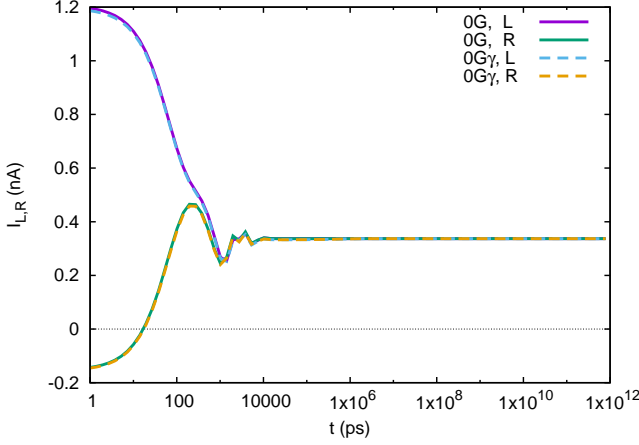


FIG. 5. The current from the left lead (L), and into the right lead (R) as a function of time for initially the vacuum state (0G), and one photon in the system (0G γ). x -polarized photons, $V_g = +2.0$ mV, $B = 0.1$ T, $\hbar\omega = 0.8$ meV, and $g_{EM} = 0.05$ meV.

(0G) that indeed the system starting in the vacuum state $|\bar{1}\rangle$ reaches quickly a steady state formed by a mixture of $|\bar{1}\rangle$ and the partial population of the two spin components of the one-electron ground state, $|\bar{3}\rangle$ and $|\bar{4}\rangle$. The lower panel of Fig. 6 shows that even when we see no changes in the current there are changes in the occupation of states. We see that due to the presence of one photon initially in the system charge is promoted temporarily to the intermediate states $|\bar{8}\rangle$ and $|\bar{9}\rangle$, that are one-electron states with approximately one photon. They are photon replicas of the two spin components of the one-electron ground state, and as such have energy 1.98 meV corresponding to one photon energy above the one-electron ground state in the bias window. We see thus, as noted

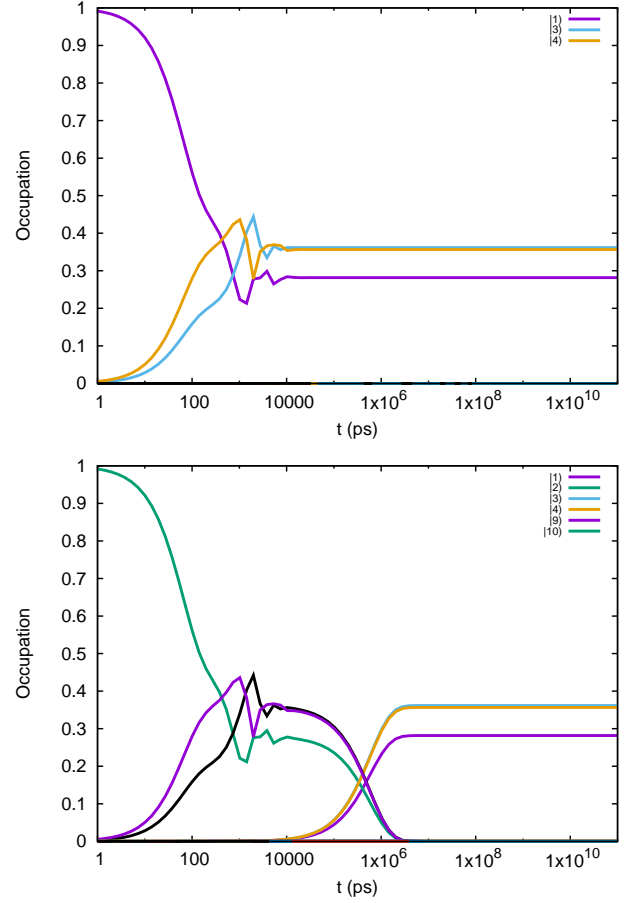


FIG. 6. The time dependent occupation of the states $|\bar{\mu}\rangle$ for initially the vacuum state (0G) (upper panel), and one photon in the system (0G γ) (lower panel). x -polarized photons, $V_g = +2.0$ mV, $B = 0.1$ T, $\hbar\omega = 0.8$ meV, and $g_{EM} = 0.05$ meV.

earlier, photon assisted tunneling into the system.²⁹ But, photons are not supplied to the system and the initial photon vanishes and the population transfers smoothly to the states $|\bar{3}\rangle$, $|\bar{4}\rangle$, and $|\bar{1}\rangle$ as before with no change seen in the current through the central system. In the far-infrared (FIR) regime the electromagnetic transitions in the system are slow so the steady state is only reached after 10 μ s. In addition, it is important to have in mind that electromagnetic transitions are only active due to the coupling to the leads, which is weak here. Without this coupling the many-body states of the central system are its eigenstates.

We now turn to more complex situations with the plunger gate voltage set at $V_g = +0.1$ and $+0.15$ mV shown in Fig. 7. For the case of $V_g = +0.1$ mV, the upper panel of Fig. 7, we see a photon replica of the singlet two-electron ground state together with the three spin components of the lowest two-electron triplet state. Just below the bias window are two one-electron states with vanishing photon components. In the lower panel of Fig. 7 we have just changed the plunger gate voltage to $+0.15$ mV in order to raise the one-electron states into the bias

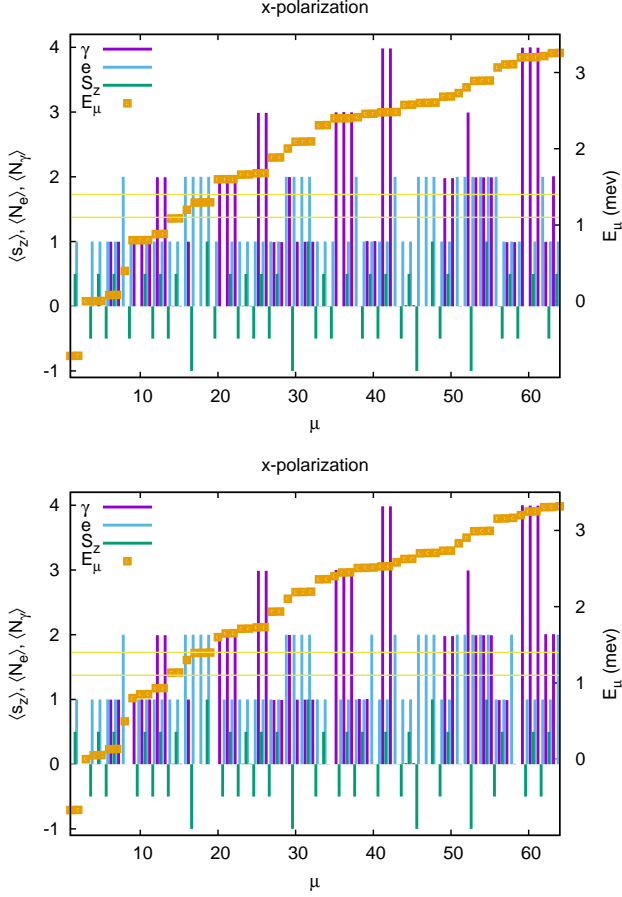


FIG. 7. The energy spectrum (right y -axis), the mean electron, the mean photon content, and the spin of the 64 lowest many-body states for $V_g = +0.1$ mV (upper panel), and $V_g = +0.15$ mV (lower panel). x -polarized photons. $\hbar\omega = 0.8$ meV, and $g_{EM} = 0.05$ meV.

window still keeping the four two-electron states there. This we do to shed light on the roles assumed by the one- and two-electrons states in our transport picture, built on sequential tunneling.

Here, we have more obvious choices for the initial state of the system. In Fig. 8 we see for the case of an initially empty system (0G), or with only one photon initially (0G γ), that the photons seem not to play any major role. The system is charged quickly to one electron, and further delayed charging seems to go in hand with the vanishing of the initial photon in the system, or if there was none in the system initially, with the appearance of a very small photon component, that again vanishes. As there are several states available below the bias window we might expect charge to get trapped in the system suppressing possible current through it in the steady state.

Before looking at the corresponding current and occupation we present in Fig. 9 the evolution of the mean electron and photon numbers for the two electrons initially in the central system, in the two-electron ground state (2G), and the first photon replica (2G γ) thereof.

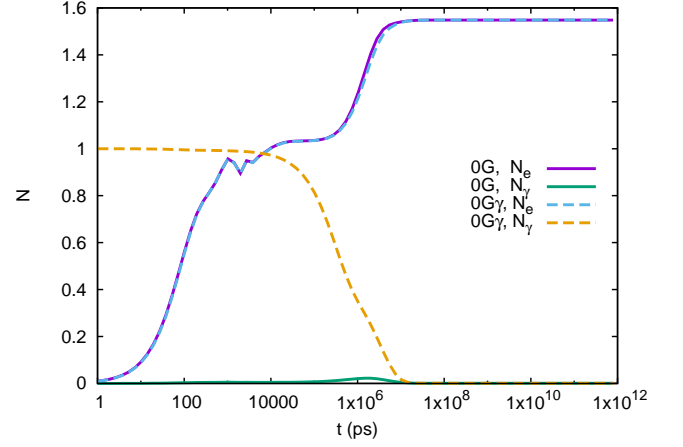


FIG. 8. Mean electron and photon numbers in the central system as a function of time for initially the vacuum state (0G), and one photon in the system (0G γ). x -polarized photons, $V_g = +0.1$ mV, $B = 0.1$ T, $\hbar\omega = 0.8$ meV, and $g_{EM} = 0.05$ meV.

Here, all changes are slow, occurring for time between

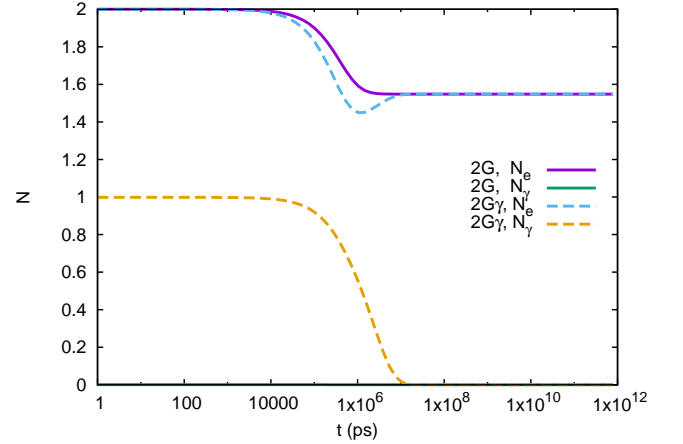


FIG. 9. Mean electron and photon numbers in the central system as a function of time for initially the two-electron ground state (2G), and the first photon replica of the two-electron ground state of the system (2G γ). x -polarized photons, $V_g = +0.1$ mV, $B = 0.1$ T, $\hbar\omega = 0.8$ meV, and $g_{EM} = 0.05$ meV.

100 ns and 10 μ s. For the first time we see here that the discharging of the system depends on the initial photon number. It is faster for the first photon replica of the two-electron ground state than for the corresponding ground state. We should have in mind that the x -polarized photon field in the system stretches the charge density into the contact area of the central system facilitating the charge to leave or enter the system.³⁰

In Fig. 10 we present the time dependent occupation of states for the case of no electron initially in the system, but either no (0G) (upper panel), or one photon

(0G γ) (lower panel), corresponding to Fig. 8. For the

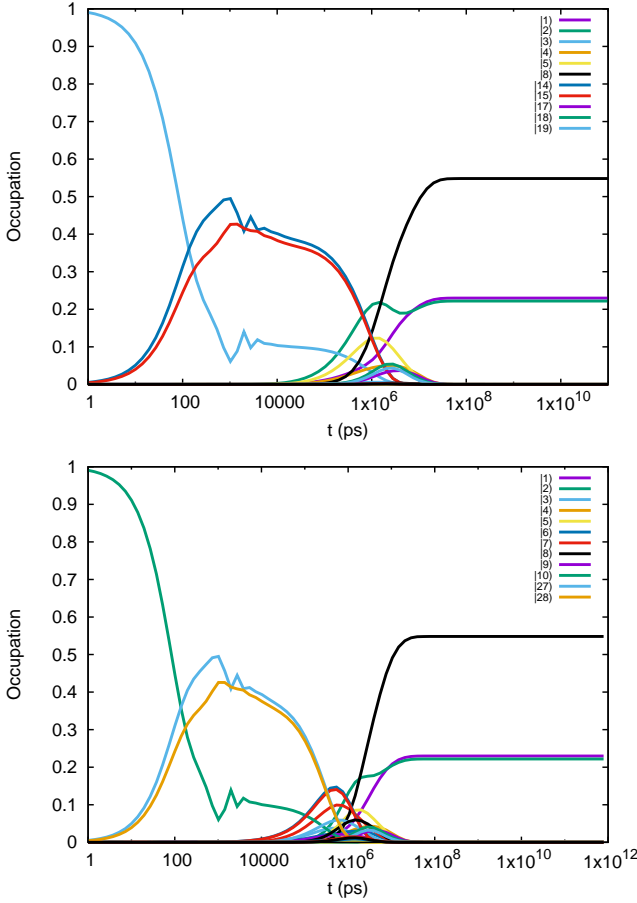


FIG. 10. The time dependent occupation of the states $|\check{\mu}\rangle$ for initially the vacuum state (0G) (upper panel), and one photon in the system (0G γ) (lower panel). x -polarized photons, $V_g = +0.1$ mV, $B = 0.1$ T, $\hbar\omega = 0.8$ meV, and $g_{EM} = 0.05$ meV.

(0G) case in the upper panel we identify the one-electron states $|\check{14}\rangle$ and $|\check{15}\rangle$ with energy $E \approx 1.08$ meV just below the bias window that are active in charging the system. The steady state is a combination of the two spin components of the one-electron ground state, and with a higher probability the two-electron ground state. The intermediate states active around $3 \mu s$ are the two-electron triplet states $|\check{17}\rangle$, $|\check{18}\rangle$, and $|\check{19}\rangle$ together with the one-electron state $|\check{5}\rangle$. All states with odd spatial parity (measured along the y -axis), that is slightly broken by the external magnetic field. As we use a state dependent coupling to the leads that depends on the spatial properties of the wave functions, the coupling of these states to the lowest subband in the leads with even parity is small.

For the (0G γ) case displayed in the lower panel of Fig. 8 we see the initial one-photon state $|\check{10}\rangle$ rapidly depopulated with the one-electron states $|\check{27}\rangle$ and $|\check{28}\rangle$ containing one photon and having energy 1.88 meV taking over. These states are the first photon replicas of the one-electron states we noticed just below the bias win-

dow. Again, we are observing a photon assisted charging of the system, and before the system reaches the same steady state as in the (0G) case we see intermediate states of two types; low energy one-electron states with no photon content like $|\check{4}\rangle$ and $|\check{5}\rangle$, and one-electron states with approximately one photon $|\check{6}\rangle$ and $|\check{7}\rangle$, and last we see small occupation of the triplet states in the bias window. So, differently from the (0G) case we see radiative transitions on the way to the steady state.

Not surprisingly, we see in Fig. 11 for $t > 200$ ps high charging current into the system. This is followed by a considerable current through the system up to $1 \mu s$ during the period it takes the system to relax on the way to the steady state. But, the final and real steady state is not fully reached until after approximately $20 \mu s$. The

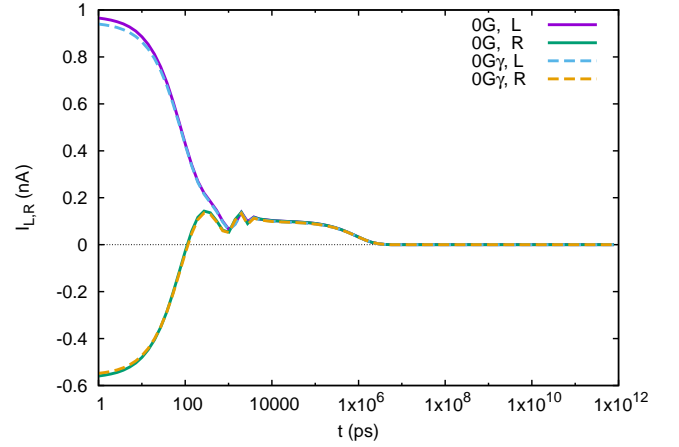


FIG. 11. The current from the left lead (L), and into the right lead (R) as a function of time for initially the vacuum state (0G), and one photon in the system (0G γ). x -polarized photons, $V_g = +0.1$ mV, $B = 0.1$ T, $\hbar\omega = 0.8$ meV, and $g_{EM} = 0.05$ meV.

logarithmic time scale in the figures can be a bit deceiving when estimating the charge flowing into and through the system. As can be confirmed by Fig. 8 approximately one electron enters the central system in the charging phase lasting to 200-500 ps, but in the intermediate time regime extending to $1 \mu s$ the number of electrons passing through is of the order of 10^5 , although on the average only 0.6 are staying in!

On the current scale used in Fig. 11 one is tempted to conclude that there is no steady state current through the system. In order to explore this situation we now analyze in more detail what happens when initially there are two electrons in the system. We started with this in Fig. 9, but now turn to the occupation (population) for the (2G) and (2G γ) cases shown in Fig. 12. The (2G) case with initially 2 electrons in the ground state is a simple case with no electromagnetic transitions active. Very slowly the two-electron ground state $|\check{8}\rangle$ (a singlet) loses charge to the two spin components of the one-electron ground state, $|\check{1}\rangle$ and $|\check{2}\rangle$. This transition is slow as the single-electron wave functions associated with these states have

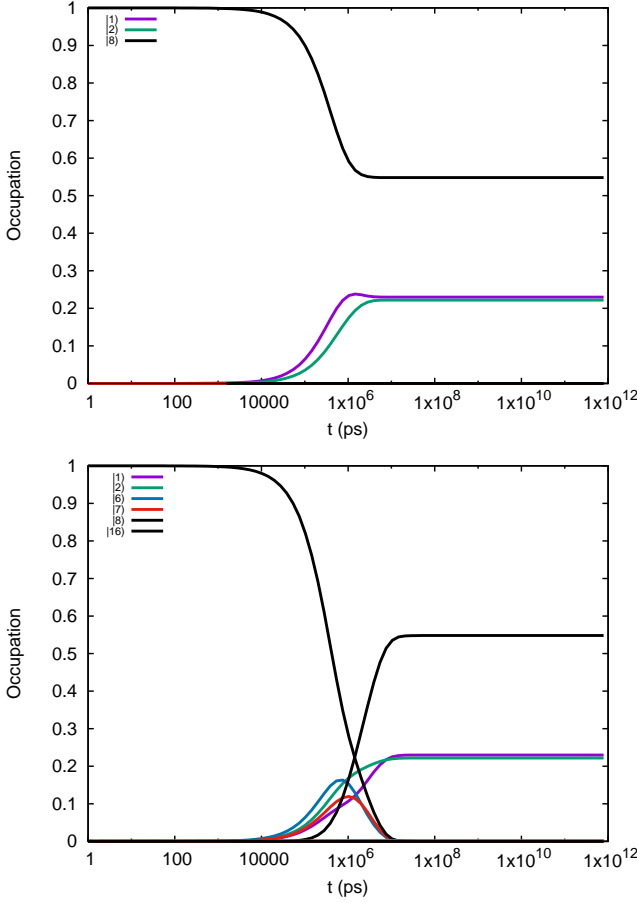


FIG. 12. The time dependent occupation of the states $|\check{\mu}\rangle$ for initially the two-electron ground state (2G) (upper panel), and the first photon replica of the two-electron ground state of the system (2G γ) (lower panel). x -polarized photons, $V_g = +0.1$ mV, $B = 0.1$ T, $\hbar\omega = 0.8$ meV, and $g_{EM} = 0.05$ meV.

a small weight in the contact area of the short wire in the central system, and all transitions are activated by the coupling to the leads, that depends on the wave functions in that region.

The relaxation of the charge from the first photon replica of the two-electron ground state $|\check{16}\rangle$ (the 2G γ case seen in the lower panel of Fig. 12) in the bias window is faster with of course the same steady state reached in the end, but now the active intermediate states are the one-electron states $|\check{6}\rangle$ and $|\check{7}\rangle$, a radiative transition terminating in the two spin components of the one-electron ground state $|\check{1}\rangle$ and $|\check{2}\rangle$.

Now, we are prepared for viewing the current into and through the system for both the cases with initially 2 electrons in the system (2G and 2G γ) displayed in Fig. 13. For the long transient regime up to $1\ \mu\text{s}$ we see the system is slowly losing charge as I_L is negative, indicating a current from the central system into the left lead, and I_R is positive indicating current from the central system into the right lead. But, we notice a *nonzero* steady state current through the system, albeit small, that we

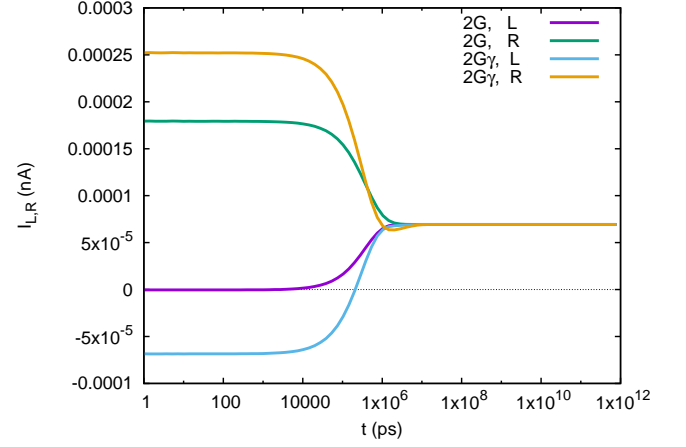


FIG. 13. The current from the left lead (L), and into the right lead (R) as a function of time for initially the two-electron ground state (2G), and the first photon replica of the two-electron ground state of the system (2G γ). x -polarized photons, $V_g = +0.1$ mV, $B = 0.1$ T, $\hbar\omega = 0.8$ meV, and $g_{EM} = 0.05$ meV.

have to analyze further. Before, we have to ask the question whether even in the case of an initially empty system (see Fig. 11) we also had this finite but small steady state current without noticing it.

Indeed, Fig. 14 confirms that there is the same steady state current through the system for the different initial cases, independent of whether we start with none, or two electrons in the system. Even, when we displace slightly the plunger gate voltage to $V_g = +0.15$ mV and thus lift the two one-electron states $|\check{14}\rangle$ and $|\check{15}\rangle$ into the bias window we continue to have a slight steady state current through the system. Where does it come from? These two one-electron states are not populated in the steady state.

The answer can be found by analyzing the partial current through each state in the system, a feature of the model that can not be repeated in experiments, but can give a valuable insight into the underlying active processes in the system. In Fig. 15 we display in the upper panel the contribution of the active one-electron states in the system, and in the lower panel the active two-electron states. In addition, we have selected states in the bias window that could be expected to carry current. In the upper panel we see that the one-electron states contribute to the charge loss from the system as we noticed earlier. The steady state current of these one-electron state seems to vanish. We have confirmed that this is indeed true. In the lower panel of Fig. 15 we notice that the steady state current is only carried by the two-electron ground state $|\check{8}\rangle$, even though it is not in the bias window. How is this possible?

As we saw earlier (see Fig. 12) the two-electron ground state is the state with the highest energy contributing significantly to the steady state. In the steady state the charge has all relaxed to states below the bias window.

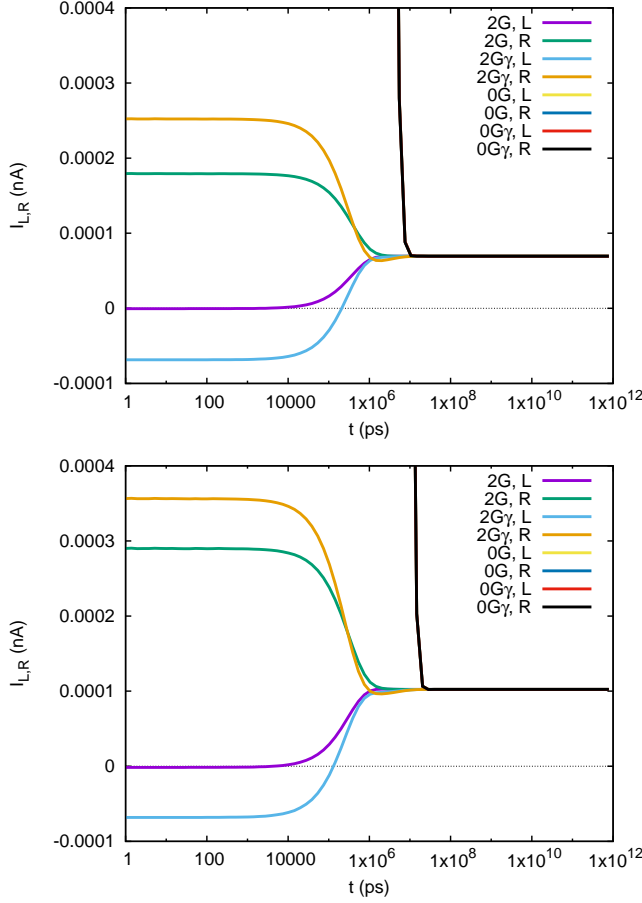


FIG. 14. Comparison of the current from the left lead (L), and into the right lead (R) as a function of time for several initial states. $V_g = +0.1$ mV (upper panel), and $V_g = +0.15$ mV (lower panel), x -polarized photons, $B = 0.1$ T, $\hbar\omega = 0.8$ meV, and $g_{EM} = 0.05$ meV.

The two-electron ground state (a spin singlet) with even parity (with respect to the y -direction) has higher coupling to the lowest subband of the leads than the spin triplet states in the bias window. We are thus seeing an off-resonance inelastic (with respect to the system lead tunneling) contribution to the steady state current by the two-electron ground state. The current is low, as it is inelastic and the coupling to the two electron state mostly confined to the parallel quantum dots is low on grounds of the geometry.

Even though we can talk about a strong electron-photon coupling here it should be stated that for the x -polarized cavity field we are well off-resonance with the photon number close to an integer for most states. For the y -polarization there is a weak Rabi-splitting for the low lying one-electron states, but not for the two-electron states, and here we used two-electron states as the initial state or started with no electrons in the central system.

The fact that electron-photon system is only in a weak resonance here can be confirmed by inspecting Figures 2, 3, and 7. All the same, it is necessary to have in mind

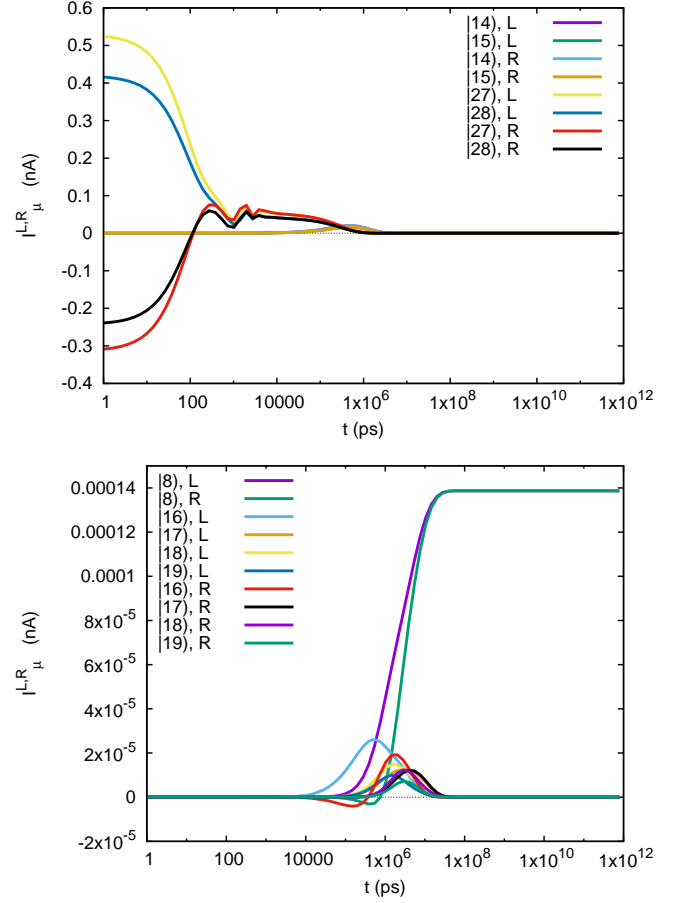


FIG. 15. The partial current carried by the state $|\tilde{\mu}\rangle$ from the left lead (L), and into the right lead (R) for the most active one-electron states (upper panel), and the most active two-electron states (lower panel). x -polarized photons, $V_g = +0.1$ mV, $B = 0.1$ T, $\hbar\omega = 0.8$ meV, and $g_{EM} = 0.05$ meV.

that even for the x -polarization here, we have dressed electron states with a mixed photon content. This is shown in Fig. 16 for the one- and two-electron ground states, ($|\tilde{1}\rangle$ and $|\tilde{8}\rangle$), and the first replica of the two-electron ground state ($|\tilde{16}\rangle$). In case of a stronger resonance between the electrons and the cavity photons we have observed in an earlier publication stronger influence of radiative transitions on the evolution of the system and stronger variations in the mean photon number.^{15,16}

III. DISCUSSION

We have used our model of electron transport through a central system with interacting electrons and photons to describe the time evolution of the system after it has been started/prepared in a certain eigenstate of the closed system. Time resolved experiments in this field have not yet been performed, but transport experiments on electron systems in photon pumped cavities are gaining strength.^{8,9} The importance of time dependent mod-

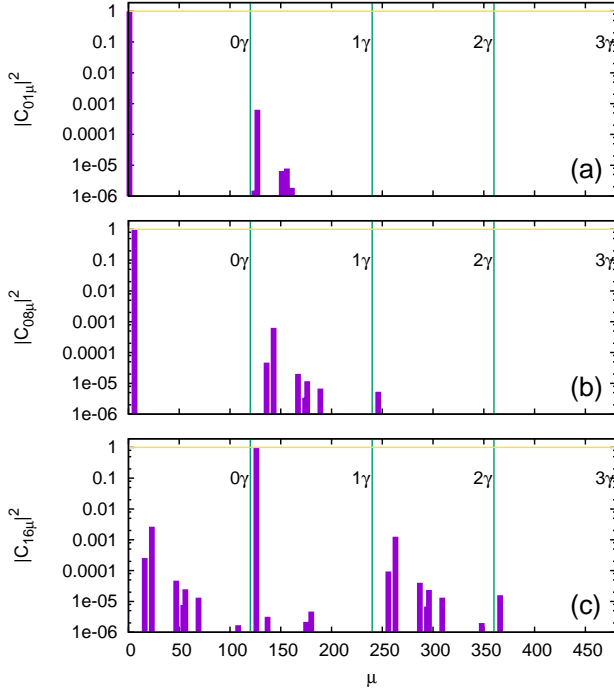


FIG. 16. Spectral composition of the one-electron ground state $|\bar{1}\rangle$ (1G) (a), the two-electron ground state $|\bar{08}\rangle$ (2G) (b), and the first photon replica of the two-electron ground state $|\bar{16}\rangle$ (2G γ) (c), in terms of a tensor product of Coulomb interacting electron states $|\mu\rangle$ and eigenstates $|n\rangle$ of the photon number operator. The photon sectors are marked by their photon number and indicated with vertical thin green lines. The unit probability is indicated with a thin yellow horizontal line. $\hbar\omega = 0.8$ meV, and $g_{EM} = 0.05$ meV.

eling of the systems is twofold: First, they allow us to gain insight into the underlying processes in the system. Second, with the knowledge of these active fundamental processes and their time evolution we can research the states of the system we would like to maintain with an external photon pumping and their relations, even in a system with a complex structure.

Accuracy in numerical calculations is essential and error can cumulate in different parts of a model evaluation. We have taken care designing all functional bases and necessary truncations thereof balancing RAM memory requirements and exactness of the results for the closed system within reasonable bounds, not shying away from heavy RAM usage. This is only feasible with heavy parallelization of the code. As we use no time-integration of the equation of motion for the long times we are interested in, we escape errors seeping in through finite time steps in an integration. Instead, we have to pay attention to the quality of the complex valued eigenvalues of the nonsymmetric Liouvillian \mathcal{L} in Eq. 12. This is a

nontrivial task and has been studied within the QuTiP python-framework.^{31,32} In our approach the accuracy of the eigenvalues and eigenvectors measured by the trace of the reduced density operator is such that the trace is always equal to 1 with at least 8 accurate figures for all the cases described here, evaluated with double precision in FORTRAN. We only notice a deviation from this level of accuracy if we attempt a calculation with no states in the bias window defined by the chemical potentials of the left and right external leads.

Only 84 points, exponentially distributed on the time-axis, are used in the figures to conserve computational time. A careful study of the details of the relaxation of the spin components forming a braided pattern, for example in Figure 6 in the range $300 < t < 10000$ ps, would require more points.

As expected, resonant tunneling through the lowest states of the central system quickly bring it into a steady state. The situation becomes more complex if the bias window defined by the external leads is located higher in the many-body energy spectrum. Then the character of the states in the window and below it, shaped by their geometry and the coupling between the constituents of the system, are of importance. In these cases we find small but important off-resonance current through the system.

We observe that even when the system, judged from the transport current through it, seems to have reached a steady state there still can be slow internal processes at work bringing it into the real (final) steady state. (See, for example, Figures 5 and 6)

From our modeling efforts it is clear that the character of the transport into and through the system is highly tunable with, or strongly depends on, the plunger gate voltage and the photon frequency of the cavity. This fact underlines the importance of a computationally effective approach to explore the dynamic properties of the system,¹⁶ and the possibility to enhance further the description of the details of the underlying physical processes beyond the presently implemented sequential tunneling to high order.

ACKNOWLEDGMENTS

This work was financially supported by the Research Fund of the University of Iceland, the Icelandic Research Fund, grant no. 163082-051, and the Icelandic Instruments Fund. We also acknowledge support from the computational facilities of the Nordic High Performance Computing (NHPC), and the Nordic network NANOCONTROL, project no.: P-13053. HSG acknowledges support from MOST, Taiwan, under grant no. 103-2112-M-002-003-MY3.

* vidar@hi.is

† goan@phys.ntu.edu.tw

[†] cstang@nuu.edu.tw

[§] manoles@ru.is

- ¹ Y.-Y. Liu, K. D. Petersson, J. Stehlik, J. M. Taylor, and J. R. Petta, *Phys. Rev. Lett.* **113**, 036801 (2014).
- ² K. D. Petersson, L. W. McFaul, M. D. Schroer, M. Jung, J. M. Taylor, A. A. Houck, and J. R. Petta, *Nature* **490**, 380 (2012).
- ³ J. J. Viennot, M. C. Dartailh, A. Cottet, and T. Kontos, *Science* **349**, 408 (2015).
- ⁴ T. Frey, P. J. Leek, M. Beck, A. Blais, T. Ihn, K. Ensslin, and A. Wallraff, *Phys. Rev. Lett.* **108**, 046807 (2012).
- ⁵ H. Toida, T. Nakajima, and S. Komiyama, *Phys. Rev. Lett.* **110**, 066802 (2013).
- ⁶ G.-W. Deng, D. Wei, J. R. Johansson, M.-L. Zhang, S.-X. Li, H.-O. Li, G. Cao, M. Xiao, T. Tu, G.-C. Guo, H.-W. Jiang, F. Nori, and G.-P. Guo, *Phys. Rev. Lett.* **115**, 126804 (2015).
- ⁷ X. Mi, J. V. Cady, D. M. Zajac, J. Stehlik, L. F. Edge, and J. R. Petta, *arXiv:1610.05571* (2015).
- ⁸ M. Delbecq, V. Schmitt, F. Parmentier, N. Roch, J. Viennot, G. Fève, B. Huard, C. Mora, A. Cottet, and T. Kontos, *Phys. Rev. Lett.* **107**, 256804 (2011).
- ⁹ L. E. Bruhat, J. J. Viennot, M. C. Dartailh, M. M. Desjardins, T. Kontos, and A. Cottet, *Phys. Rev. X* **6**, 021014 (2016).
- ¹⁰ L. P. Kouwenhoven, S. Jauhar, J. Orenstein, P. L. McEuen, Y. Nagamune, J. Motohisa, and H. Sakaki, *Phys. Rev. Lett.* **73**, 34433446 (1994).
- ¹¹ U. Hohenester, *Phys. Rev. B* **81**, 155303 (2010).
- ¹² C. Bergenfeldt and P. Samuelsson, *Phys. Rev. B* **87**, 195427 (2013).
- ¹³ T. L. van den Berg, C. Bergenfeldt, and P. Samuelsson, *Phys. Rev. B* **90**, 085416 (2014).
- ¹⁴ V. Gudmundsson, A. Sitek, P. yi Lin, N. R. Abdullah, C.-S. Tang, and A. Manolescu, *ACS Photonics* **2**, 930934 (2015).
- ¹⁵ V. Gudmundsson, T. H. Jonsson, M. L. Bernodussen, N. R. Abdullah, A. Sitek, H.-S. Goan, C.-S. Tang, and A. Manolescu, *Ann. Phys.*, in press (2016), *arXiv:1605.08248*.
- ¹⁶ T. H. Jonsson, A. Manolescu, H.-S. Goan, N. R. Abdullah, A. Sitek, C.-S. Tang, and V. Gudmundsson, *ArXiv e-prints* (2016), *arXiv:1610.03223* [cond-mat.mes-hall].
- ¹⁷ J. Marino and S. Diehl, *Phys. Rev. B* **94**, 085150 (2016).
- ¹⁸ O. Jonasson, C.-S. Tang, H.-S. Goan, A. Manolescu, and V. Gudmundsson, *Phys. Rev. E* **86**, 046701 (2012).
- ¹⁹ V. Gudmundsson, O. Jonasson, T. Arnold, C.-S. Tang, H.-S. Goan, and A. Manolescu, *Fortschritte der Physik* **61**, 305 (2013).
- ²⁰ O. Jonasson, C.-S. Tang, H.-S. Goan, A. Manolescu, and V. Gudmundsson, *New Journal of Physics* **14**, 013036 (2012).
- ²¹ V. Gudmundsson, A. Sitek, N. R. Abdullah, C.-S. Tang, and A. Manolescu, *Annalen der Physik* **528**, 394403 (2016).
- ²² V. Moldoveanu, A. Manolescu, and V. Gudmundsson, *New Journal of Physics* **11**, 073019 (2009).
- ²³ V. Gudmundsson, C. Gainar, C.-S. Tang, V. Moldoveanu, and A. Manolescu, *New Journal of Physics* **11**, 113007 (2009).
- ²⁴ S. Nakajima, *Prog. Theor. Phys.* **20**, 948 (1958).
- ²⁵ R. Zwanzig, *J. Chem. Phys.* **33**, 1338 (1960).
- ²⁶ W. Weidlich, *Zeitschrift für Physik* **241**, 325 (1971).
- ²⁷ R. Nakano, N. Hatano, and T. Petrosky, *International Journal of Theoretical Physics* **50**, 11341142 (2010).
- ²⁸ T. Petrosky, *Progress of Theoretical Physics* **123**, 395420 (2010).
- ²⁹ N. R. Abdullah, C.-S. Tang, A. Manolescu, and V. Gudmundsson, *Physica E: Low-dimensional Systems and Nanostructures* **64**, 254262 (2016).
- ³⁰ N. R. Abdullah, C.-S. Tang, A. Manolescu, and V. Gudmundsson, *Journal of Physics: Condensed Matter* **28**, 375301 (2016).
- ³¹ P. D. Nation, J. R. Johansson, M. P. Blencowe, and A. J. Rimberg, *Phys. Rev. E* **91**, 013307 (2015).
- ³² J. Johansson, P. Nation, and F. Nori, *Computer Physics Communications* **184**, 12341240 (2013).